Planetary and Space Science 113-114 (2015) 264–274

Contents lists available at ScienceDirect

Planetary and Space Science

journal homepage: www.elsevier.com/locate/pss

Hydrogen halides measurements in the Venus mesosphere retrieved from SOIR on board Venus express

A. Mahieux [a,b,*], V. Wilquet [a], A.C. Vandaele [a], S. Robert [a], R. Drummond [a], S. Chamberlain [a], A. Grau Ribes [c], J.L. Bertaux [d,e]

[a] Planetary Aeronomy, Belgian Institute for Space Aeronomy, 3 av. Circulaire, B-1180 Brussels, Belgium
[b] Fonds National de la Recherche Scientifique, 5 rue d'Egmont, B-1000 Brussels, Belgium
[c] Université Libre de Bruxelles, Faculté des Sciences, 50 av. F. Roosevelt, Brussels, Belgium
[d] LATMOS, 11 Bd d'Alembert, 78280 Guyancourt, France
[e] Institut Pierre Simon Laplace, Université de Versailles-Saint-Quentin, 78280 Guyancourt, France

ARTICLE INFO

Article history:
Received 12 March 2014
Received in revised form
9 September 2014
Accepted 4 December 2014
Available online 17 December 2014

Keywords:
Planetary atmosphere
Venus
Composition
HCl
HF
Isotopic ratio

ABSTRACT

The SOIR instrument on board Venus Express regularly sounds the Venus mesosphere using the solar occultation technique. Densities and volume mixing ratios of HCl and HF are measured in the 70–115 km and 75–110 km altitude region respectively, at the Venus terminator. All latitudes from pole to pole are covered. In this work, we study the latitude and long-term variations of the volume mixing ratio (VMR) of HCl, and the long-term time trend of HF, from June 2006 to February 2013. This period of time corresponds to approximately eleven Venusian years. Large variations in the VMR profiles are observed, mostly on the short-term. Both hydrogen halides present unforeseen positive exponential gradients of their VMR with pressure, which shows time and latitude variations. Long-term trends on the whole period of the HCl VMR are also observed at certain pressure levels in the equatorial and polar regions. HF also presents a time dependence of its VMR at certain pressure levels. Results are compared to previous HCl and HF VMR observations. The ability of SOIR to target both $H^{35}Cl$ and $H^{37}Cl$ isotopologues has also been investigated. Numerous concomitant density profiles lead to the determination of the $^{37}Cl/^{35}Cl$ isotopic ratio on Venus, found to be equal to 0.34 ± 0.13, which is compatible with the value found on Earth.

© 2014 Elsevier Ltd. All rights reserved.

1. Introduction

Hydrogen halides play an important role in the chemistry of the Venus atmosphere, being active species involved in three of the main chemical cycles, that is, the CO_2, the sulfur oxidation and the polysulfur cycles. Reviews of these chemical reactions can be found in Krasnopolsky (2012b), McElroy et al. (1973), Mills and Allen (2007), Prinn (1971) and Yung and DeMore (1982), for example. They all identified HCl as being a key constituent for which further observations are important to better understand the chemistry of the Venus thermosphere.

HCl has first been observed in the Venus atmosphere by Connes et al. (1967), who reported volume mixing ratio values at the cloud top as being 0.6 ppmv. The HCl value was lately corrected by Young (1972) as being equal to 0.4 ± 0.07 ppmv. Since then, Iwagami et al. (2008) observed an HCl mixing ratio of 0.76 ± 0.1 ppmv at 61–67 km. Krasnopolsky (2010) measured HCl abundance of 0.40 ± 0.03 ppmv at 74 km, using the CSHELL spectrograph at NASA IRTF. Sandor and Clancy (2012) reported HCl vertical profiles with a mixing ratio of 0.4 ppmv near 70 km decreasing to 0.2 ppmv and less near 90 km.

HF has also first been observed in the Venus atmosphere by Connes et al. (1967), with a mixing ratio at the cloud top of 5 ppbv. Krasnopolsky (2010) reported values of the abundance of 3.5 ± 0.2 ppbv at 68 km.

The SOIR instrument performs regular observations of the Venus mesosphere on a 24 Earth hours basis at the Venus terminator, covering all latitudes, and measures HCl and HF concentration, among other species, such as CO_2 (Mahieux et al., 2014a; Mahieux et al., 2012), CO (Vandaele et al., 2014), H_2O and HDO (Fedorova et al., 2008), SO_2 (Belyaev et al., 2012; Mahieux et al., 2014b) and the aerosol loading in the upper haze (Wilquet et al., 2012; Wilquet et al., 2009).

This paper describes the SOIR hydrogen halides dataset, focusing on the latitude variations of HCl and the long-term variations of HCl and HF between June 2006 and February 2013.

* Corresponding author at: Planetary Aeronomy, Belgian Institute for Space Aeronomy, 3 av. Circulaire, B-1180 Brussels, Belgium.
E-mail address: arnaud.mahieux@aeronomie.be (A. Mahieux).

http://dx.doi.org/10.1016/j.pss.2014.12.014
0032-0633/© 2014 Elsevier Ltd. All rights reserved.

2. Instrument and measurement description

The SOIR (Solar Occultation in the InfraRed) instrument has been designed to measure infrared (IR) spectra of the Venus atmosphere using the solar occultation technique (Nevejans et al., 2006). This method derives unique information on the vertical composition and structure of the mesosphere and lower thermosphere at the terminator (Mahieux et al., 2010, 2012, 2014a, 2014b; Vandaele et al., 2008, 2014). SOIR is an extension mounted on top of the SPICAV instrument (Bertaux et al., 2007). SPICAV/SOIR is one of the seven instruments on board Venus Express, a planetary mission of the European Space Agency (ESA) that was launched in November 2005 and inserted into orbit around Venus in April 2006 (Titov et al., 2006).

The instrument has already been extensively described in previous publications (Mahieux et al., 2008, 2009; Nevejans et al., 2006; Vandaele et al., 2013) and will only be briefly outlined here. SOIR is an Echelle grating spectrometer operating in the near-IR, combined with an acousto-optic tunable filter (AOTF) for the selection of the wavenumber interval to be recorded. The covered spectral domain ranges from 2257 to 4430 cm^{-1} (2.29 to 4.43 μm) and is divided into 94 diffraction orders (from 101 to 194). The limits of these diffraction orders are given in Vandaele et al. (2013). The bandwidth of the AOTF was originally designed to be 20 cm^{-1}, as measured on ground before launch, to allow light from only one order to reach the echelle grating. However, the measured bandwidth of SOIR is approximately 24 cm^{-1} (Mahieux et al., 2010) and the transfer function presents non-negligible side lobes: as a consequence, information from adjacent orders leaks onto the detector. To account for it, seven contiguous diffraction orders are usually simulated, that is, the targeted one and the three directly higher and lower adjacent orders.

The resolution of SOIR varies with the diffraction order, with values of about 0.11 cm^{-1} and 0.21 cm^{-1} in orders 101 and 194 respectively. The SOIR detector is composed of 320 pixels in its spectral direction. The spectral width of a pixel varies from 0.06 to 0.12 cm^{-1} and the free spectral range has a constant value of 22.4 cm^{-1}. In the spatial direction of the detector, 24 rows are fully illuminated, and are combined on-board into two groups of 12 rows called hereafter bins. Two simultaneous measurements are thus obtained at two slightly different altitudes, due to the small inclination of the instrument slit with respect to the Venus limb. SOIR can measure up to four diffractions orders each occultation, with a maximum integration time of 250 ms per diffraction order.

SOIR performs solar occultation observations of the Venus atmosphere from a polar orbit with its periapsis located above the North Pole. All latitudes are well covered on both sides of the terminator, except for the 30°–60° North region, due to the geometry of the spacecraft orbit. The vertical resolution, that is, the vertical altitude range sounded by the projected slit at the limb on the atmosphere at the time of a measurement, varies from a few hundreds of meters for measurements at the North Pole to approximately 5 km when reaching the South Pole. The vertical sampling, that is, the vertical distance between the mean altitude of two successive soundings, is also latitude-dependent, having values of approximately 2 km close to the North Pole, ~500 m between 40° and 70° North, and rising up to 5 km close to the South Pole. The maximum altitude range probed by SOIR varies from 65 km up to 170 km. For HCl, the typical altitude of detection extends from 70 to 115 km and for HF from 75 to 110 km at maximum. The lower boundaries correspond to the atmospheric saturation of the lines in the SOIR spectra, while the upper boundary is linked to the detection of the strongest band in the selected SOIR wavenumber range. The occultations are grouped in occultation seasons (OS), which are time periods when solar occultations occur as seen from the VEX spacecraft. These OS periods occur roughly every three months for one to two months.

The spectroscopic parameters were obtained from HITRAN 2012 (Rothman et al., 2013). Values of the pressure broadening coefficients and shifts were corrected to take into account that the atmosphere of Venus is mainly composed of CO_2 instead of nitrogen and oxygen as on Earth (Toth and Darnton, 1974; Tudorie et al., 2012; Vandaele et al., 2008). For HCl, the 1–0 transitions of both isotopologues $H^{35}Cl$ and $H^{37}Cl$ absorb in the 2815 to 3043 cm^{-1} region (orders 126 to 135). The 1–0 transition of the main isotopologue of HF is observed in the 3933 to 4125 cm^{-1} region (orders 176 to 183).

3. Retrieval method

The number density profiles are calculated using the ASIMAT algorithm that has been described in previous publications, see Mahieux (2010, 2011, 2012, 2014a, 2014b), Vandaele et al. (2014). It will be summarized here.

The method determines the number density, temperature and aerosol extinction profiles using an iterative procedure. At each iteration, number density profiles are determined using the Bayesian Optimal Estimation method (Rodgers, 2000) implemented in an onion peeling frame. Considering separately all diffraction orders measured during one occultation, the logarithm of the number density of the different species and the baseline (modeled as a 5th-order polynomial) are adjusted as a function of altitude (Mahieux et al., 2010). The algorithm takes the saturation of atmospheric lines into account, and only spectra with unsaturated lines of the weakest simulated vibrational bands are considered (Mahieux et al., 2014a). The temperature profile is not fitted at this level. In the retrieval algorithm, the a-priori number densities are taken from an modified VIRA model (Venus International Reference Atmosphere model) from Hedin et al. (1983), Zasova et al. (2007). The a-priori HCl and HF VMRs are taken constant with altitude and equal to 1 ppmv and 300 ppbv respectively. The covariance on the density value is taken as 25% of the a-priori number density logarithm. In the retrieval, the vertical resolution is accounted for by considering a multiple ray tracing across the SOIR field of view, typically 24 rays equally widespread are taken into account (Mahieux et al., 2014a). A known drawback of the Bayesian algorithm is their dependence to the a-priori profiles. To limit this dependence, only the number density values that were actually fitted for each profile are taken into account: this number is given by the degrees of freedom (DOF) of the retrieval extracted from the Rodgers averaging kernel matrix. The DOF is equal to the trace of the averaging kernel matrix, and indicates the total number of independent variables that can be derived from the set of spectra. We only consider the layers corresponding to the DOF largest eigenvalues of the averaging kernel matrix (Mahieux et al., 2014a, 2014b).

This step is part of the global iterative process which deals with the combination of the number density profiles obtained independently from the different orders and with the determination of the temperature profile. The absorption cross sections are indeed temperature-dependent in the infrared domain. The temperature profile is determined using the hydrostatic equilibrium applied on the CO_2 density profile, which is being measured during the same occultation. An assumption has to be made at the top of the profile and is derived from VAST (Venus Atmosphere from SOIR measurements at the Terminator), described in Mahieux et al. (2012, 2014a). The temperature is derived from CO_2 only in the heterosphere, and from the total number density in the homosphere, thus accounting for the CO_2 volume mixing ratio (VMR), which is taken from VIRA. The final profile of one particular species is built by applying a moving average on all individual local number density values, weighted by their uncertainties (Mahieux et al.,

2012). During the retrieval process, the vertical box width of the moving average function is equal to ± 2 scale heights. Although profiles with narrower box width are also generated, the box of ± 2 scale heights width is used for checking the convergence. The final grid corresponds to a 1 km altitude step scale. This two steps procedure, that is, the determination of the number density profiles from the eight spectral orders, and the combination of the profiles and determination of the hydrostatic temperature profile, is done in an iterative scheme. Convergence is achieved when all the density and temperature profiles stabilize, that is, remain within the uncertainty of the previous iteration. It usually occurs in three to four steps.

The outputs of this procedure are the number density, temperature, pressure, total number density, total mass density and volume mixing ratio profiles. The volume mixing ratio profiles are directly calculated using the CO_2 number density profile obtained from the same occultation set of spectra. The only quantity that needs to be assumed is the CO_2 VMR profile. For occultations during which CO_2 was not observed (no order where CO_2 absorbs was measured), the HCl and HF VMRs are calculated using the total density profile of VAST. In the following, only VMR profiles that were directly calculated using CO_2 derived from the SOIR spectra will be presented.

4. Results and discussion

4.1. Dataset description

In the present work, the dataset covering the June 2006 to February 2013 period has been investigated, covering approximately 11 Venusian years. For $H^{35}Cl$ and $H^{37}Cl$, 180 orbits are considered; their localization is presented in panel A of Fig. 1. HF was measured in 44 orbits, and the maps showing where the observations occurred are presented in panel B of the same figure. The 25 first OS are covered in this study. Fourteen orbits, out of all the orbits during which HCl was observed, were rejected for $H^{35}Cl$ because of low signal to noise ratio. For $H^{37}Cl$, 19 orbits were rejected for the same reason. Seven orbits from HF could not be correctly fitted and are not presented in this work.

4.2. Hydrochloric acid

The ASIMAT algorithm was used to derive the $H^{35}Cl$ and $H^{37}Cl$ number density profiles for the entire database described above. To illustrate the good quality of the $H^{35}Cl$ and $H^{37}Cl$ results, the spectral fit of four spectra, recorded in order 130 (2905–2930 cm^{-1}) during orbit 341.1 (28/03/2007, 82°N, 6 PM) are presented in Fig. 2, for different altitude levels (102.1 km, 91.5 km, 82.5 km and 73.4 km). In this order, two lines from the main isotopologue and one line of the second coming from order 130 are seen (R(0) of $H^{35}Cl$ at 2906.3 cm^{-1}, R(1) of $H^{35}Cl$ at 2925.9 cm^{-1} and R(1) of $H^{37}Cl$ at 2923.7 cm^{-1}). The other lines that are seen out of the noise are coming from adjacent orders (R(0) of $H^{37}Cl$ from order 129, R(2) of $H^{37}Cl$ and R(2) of $H^{37}Cl$ from order 131, R(3) of $H^{37}Cl$ and R(3) of $H^{37}Cl$ from order 132).

All number density profiles are presented in panels A ($H^{35}Cl$) and B ($H^{37}Cl$) of Fig. 3 as a function of the total pressure; the approximate altitude is also given in correlation with the pressure scale. They cover the 70 to 115 km altitude region. The HCl density vertical profiles that are presented here have been calculated for a width of the moving average box equal to ± 0.4 scale heights (see the definition in the Retrieval method section). In these plots, the color is the absolute latitude (blue for equatorial, red for polar measurements). The SOIR HCl density profiles are compared with a profile obtained with the photochemical model of Krasnopolsky (2012b), and shows a good agreement in terms of order of magnitude. The number density slope is different between the model and the SOIR measurements. The HCl VMR profiles are presented in panels C ($H^{35}Cl$) and D ($H^{37}Cl$) of the same figure. The VMR is only displayed when CO_2 and HCl were measured concurrently at the same altitude, and is obtained by dividing the HCl number densities by the total number densities, which are calculated from the concomitant CO_2 measurements. The uncertainties on both number densities and VMR range between 5% and 100%, with a mean value amongst all orbits and all altitudes of 28%. The relative error does not directly depend on the altitude level, but on the signal to noise ratio. The number densities and the VMRs are given as a function of pressure, in order to remove the total number density variability with altitude. After removing the global atmosphere time and latitude variations, large HCl VMR variations are still observed at all altitudes, up to two orders of magnitude; the average geometric standard deviation, that is, the standard deviation of an exponential variable, is equal to 32. This means that values 32 times higher or lower that the average value are encountered. As a general trend, the VMR profiles are not constant with altitude below 0.1 mbar ($\sim$92 km), a slight decrease is usually observed with decreasing altitude; above 0.1 mbar, the VMR is usually either constant or decreasing with increasing altitude.

Observations of both isotopologues are always performed simultaneously, since absorption lines of both species are observed in the same order (see order 130 in Fig. 2, for example). Therefore, combining the measurement of both isotopologues easily provides information about the $^{37}Cl/^{35}Cl$ isotopic ratio. The only limitation comes from the altitude range at which both isotopologues are measured together. Indeed since $H^{37}Cl$ is less abundant, its absorption features come out the noise of the spectra at lower altitudes, and conversely the absorption of the main isotopologue saturates at higher altitudes than that of its heavier counterpart. Results are presented in Fig. 4. One mean value of the ratio has been obtained for each individual occultation during which overlaps of the profiles of both isotopologues were observed. The average of all these individual values of the $^{37}Cl/^{35}Cl$ isotopic ratio is found to be equal to 0.34 ± 0.13, which, within error bars, is compatible with the 0.32 value found on Earth (Rothman et al., 2013).

Profiles have been grouped in latitudinal bins in order to investigate possible trends. A latitudinal symmetry relative to the Equator has been considered, together with a longitudinal symmetry with regard to the terminator side, that is, no difference between morning and evening sides of the terminator were considered in this work. These bins extend from 0°–30°, 30°–70°, 70°–80° and 80°–90°, respectively. The number of observations in the different latitude bins is summarized in Table 1. Both isotopologues have been considered together to build these profiles, since: (i) we showed that the $^{37}Cl/^{35}Cl$ isotopic ratio can be considered as equivalent to the one on Earth, (ii) the atmosphere is well mixed at altitudes below the homopause, located at an approximate pressure level of 10^{-6} mbar ($\sim$130 km) on Venus (Mahieux et al., 2012; von Zahn et al., 1980), (iii) the molecular mass difference is small between the two isotopologues. The mean values are calculated using the pressure scale, and not the altitude. The mean VMR profiles are presented in Fig. 5 for the different latitude bins; the colored envelopes are the weighted standard deviations. Corresponding altitude levels are indicated on the plot. Three regions are clearly observed. The first one, below the 4 mbar pressure level ($\sim$79 km), presents nearly constant VMR profiles in all bins (expect in the 30°–70° region where no data are available) with VMRs at 10 mbar ($\sim$74 km) varying between 29 ppbv $\pm$ 91% in the equatorial bin, 31 ppbv $\pm$ 40% in the 70°–80° bin and 55 ppbv $\pm$ 134% in the polar region. In the region between

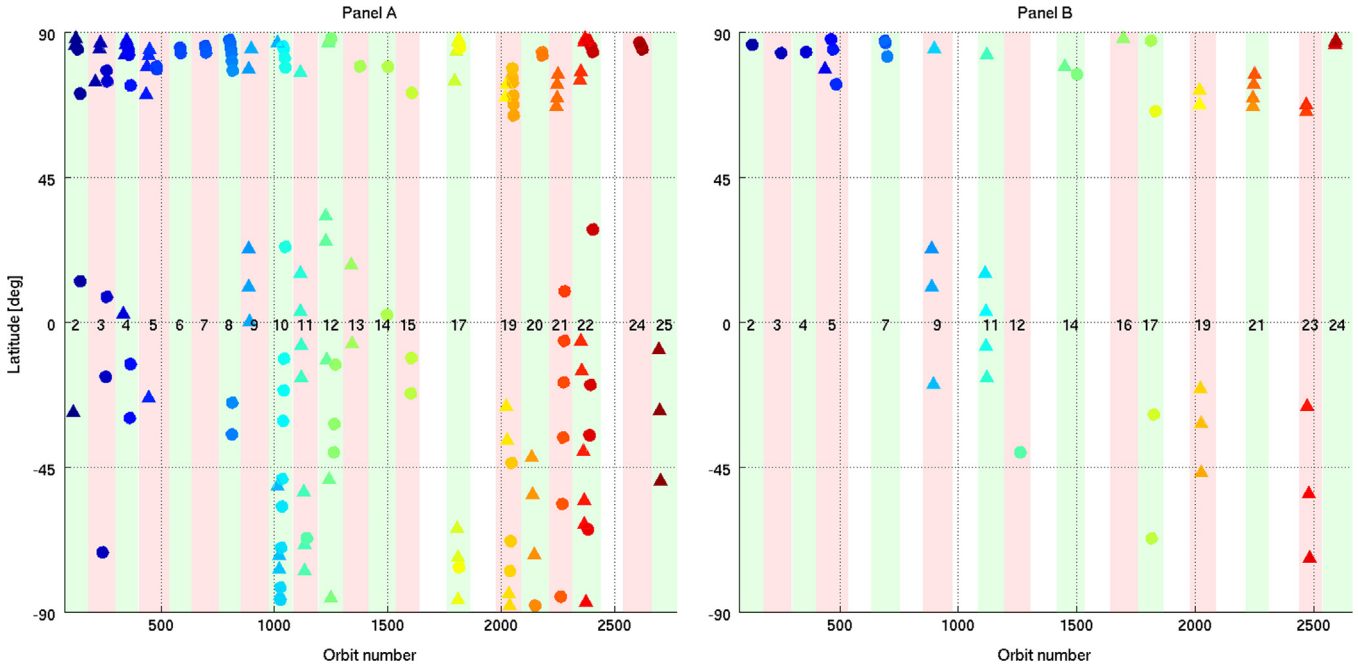

Fig. 1. Geo-localization of the orbits considered for the $H^{35}Cl$ and $H^{37}Cl$ (Panel A) and HF (Panel B) study, orbit number as a function of latitude. The numbers at the zero latitude level are the occultation season numbers. In all panels, circles are for morning measurements, while triangles are for evening ones. The color code is the orbit number.

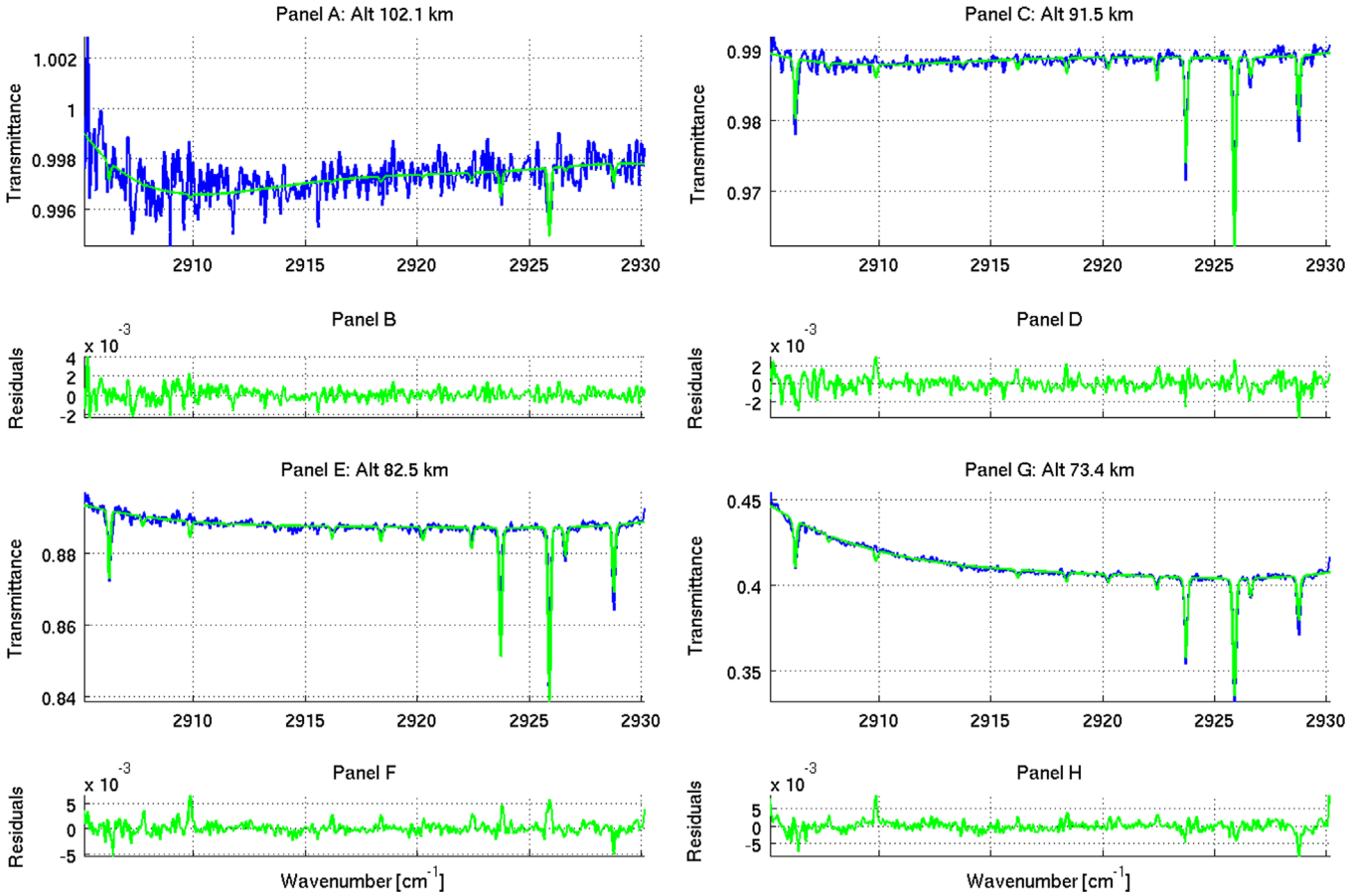

Fig. 2. Example of spectral fit for orbit 341.1 (28/03/2007) at four altitude levels (102.1 km in Panel A, 91.5 km in Panel C, 82.5 km in Panel E and 73.4 km in Panel G). In these panels, the measured spectra (order 130 bin 1) are in blue and the fitted spectra are in green. In Panels B, D, F and H, the residuals of the fits are plotted, corresponding respectively to Panels A, C, E and G.

the 1 mbar (~84 km) and 0.01 mbar (~102 km) pressure levels, the exponential increase of the VMR with rising altitude is clearly seen in the plots for all latitude bins. Above the 0.02 mbar level (~98 km), the VMRs are nearly constant again; the VMRs at 0.01 mbar (~102 km) are equal to 0.8 ppmv ± 31% in the equatorial bin, 1 ppmv ± 49% in the mid-latitude bin, 0.5 ppmv ± 44% in

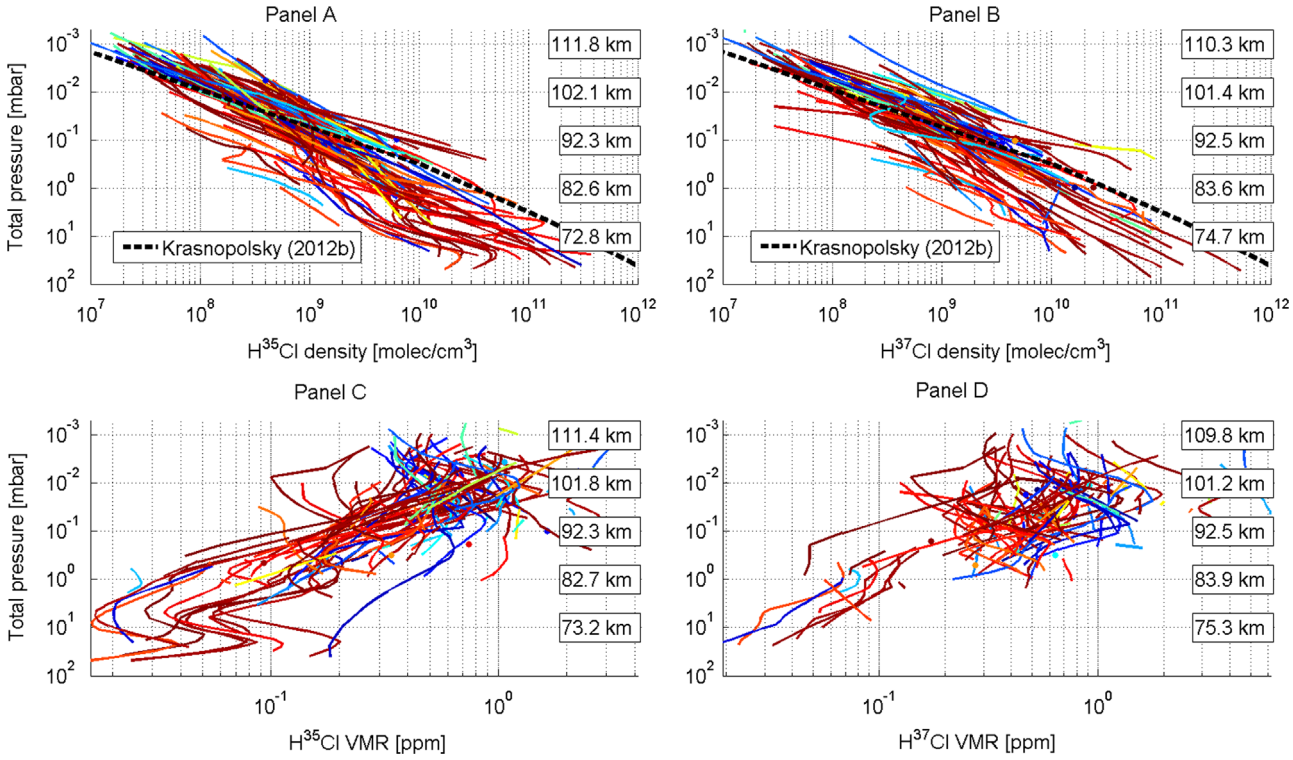

Fig. 3H. ^{35}Cl and $H^{37}Cl$ number density profiles (panels A and B respectively) and VMR profiles (panels C and D). The density and VMR profiles are given as a function of pressure level. The VMR profiles are only calculated at altitudes where the total density could be inferred from the CO_2 density. The altitude is also shown in correlation with the pressure scale. The color code is the absolute latitude (blue to red for increasing absolute latitude). The error bars are not displayed for sake of clarity. They vary between 5% and 100%, with an average value of 28%. The density profiles are compared with a number density profile derived from the photochemical model of Krasnopolsky (2012b).

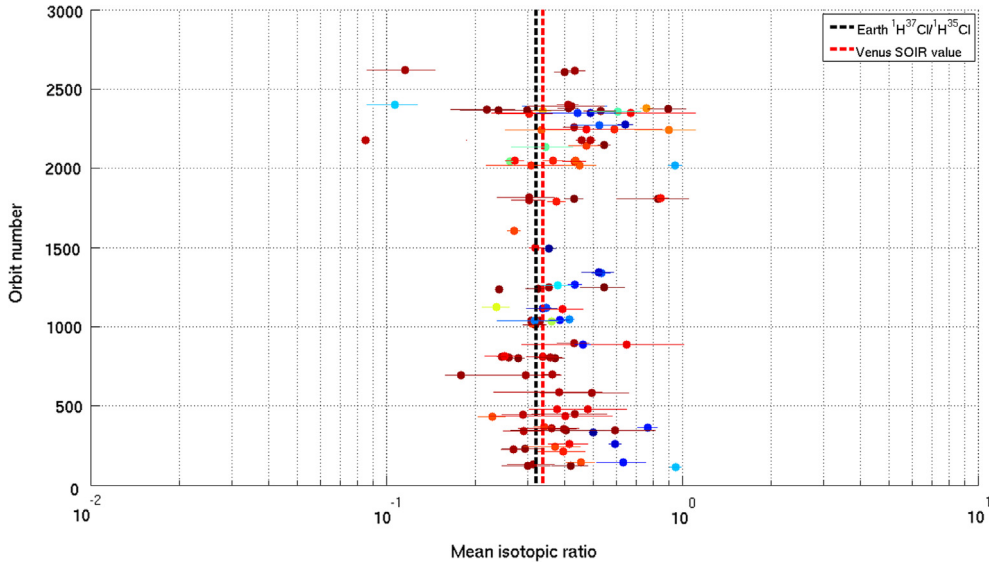

Fig. 4. Mean $^{37}Cl/^{35}Cl$ isotopic ratio for all simultaneous measurements of $H^{37}Cl$ and $H^{35}Cl$, together with its uncertainty. The color code is the absolute latitude, bluish values for equatorial measurements, reddish for polar. The black vertical line is the Earth mean $^{37}Cl/^{35}C$ isotopic ratio of 0.3198, from Rothman et al. (2013), and the red one is the global mean value calculated from the profiles, found to be equal to 0.34 ± 0.13.

Table 1
Sample for each latitude bin of HCl.

Latitude bin	Number of measurements $H^{35}Cl$	Number of measurements $H^{37}Cl$	Latitudinal density of observations $H^{35}Cl$ [measurements per degree]	Latitudinal density of observations $H^{35}Cl$ [measurements per degree]
0–30°	37	37	1.2	1.2
30–70°	32	30	0.8	0.8
70–80°	34	33	3.4	3.3
80–90°	63	61	6.3	6.1

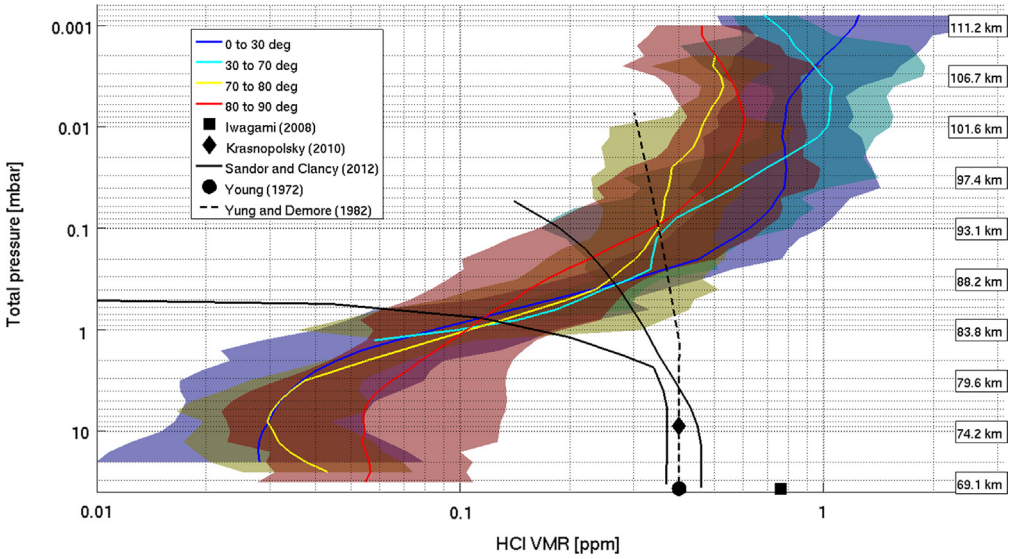

Fig. 5. Mean value of the $H^{35}Cl$ and $H^{37}Cl$ VMR for the different latitude bins defined in Table 1 as a function of total pressure. The altitude is also shown in correlation with the pressure scale. The weighted standard deviations are the colored shaded envelopes. The profiles are compared to literature data (Iwagami et al., 2008; Krasnopolsky, 2012b; Sandor and Clancy, 2012; Young, 1972; Yung and DeMore, 1982).

the 70°–80° bin and 0.6 ppmv ± 33% in the polar bin. These values have been compared to data from the literature. Nightside values reported by Sandor and Clancy (2012) are of the same order of magnitude, but completely disagree on the shape of the profiles: they observed constant VMRs below the 10 mbar level (~74 km) and are one order of magnitude larger than all the profiles reported in this work. Above that pressure level, a negative gradient with decreasing pressure was reported by Sandor and Clancy, whereas the SOIR data show a clear positive gradient for all latitude bins. The agreement with the model of Yung and DeMore (1982) is not good either, as they reported a constant VMR below the 1 mbar level (~84 km) which is one order of magnitude larger than the SOIR VMRs; their VMR profile is slightly decreasing with decreasing pressure and reaches values in agreement with SOIR data above the 1 mbar pressure level (~84 km). Literature data from Iwagami et al. (2008), Young (1972) and Krasnopolsky (2010) measured above the cloud top at altitudes varying between 70 and 74 km are also one order of magnitude larger than the SOIR mean values reported in this work. However, in contrast to the SOIR data, measurements found in the literature were not taken at the terminator. Also, results from photochemical models, such as Krasnopolsky (2012b), usually suggest constant HCl VMR profiles in the altitude region where SOIR is sensitive.

Finally, the long-term variations are addressed for two selected latitude regions: the 0°–30° and 80°–90° bins, for which a large enough number of profiles is available, see Table 1. They are presented in Figs. 6 and 7 respectively. In these figures, the $H^{35}Cl$ and $H^{37}Cl$ VMR are given for four pressure levels (0.01 mbar or ~102 km, 0.03 mbar or ~97 km, 0.1 mbar or ~93 km and 0.32 mbar or 88 km), together with their uncertainty. At the Equator, the short-term variations, that is, the variations from orbit to orbit, at 0.1 mbar (102 km) are of a factor 2 during the period between orbits 1 (May 2006) and 1800 (April 2011) and show a large increase up to one order of magnitude afterwards. The same is observed at 0.03 mbar and 0.1 mbar (~97 km and ~93 km). At the largest pressure level, 0.32 mbar (~88 km), a constant exponential increase over the whole period is observed, with exponential trends values varying from 0.193 ± 0.005 ppmv in August 2006 to 0.56 ± 0.02 ppmv in February 2013, or a factor close to 3. It should also be underlined that the amplitudes of these long-term variations, that is, the general trend over the whole period, are much smaller than the ones of the short-term variations (Krasnopolsky, 2012b).

In the polar regions, a slightly different situation is observed. The variations are presented in Fig. 7 for the same four pressure levels as in the equatorial region. At all pressure levels, an exponential increase is observed between orbits 1 and 900 (August 2006 and October 2008). We evaluated the variations for the 4 pressure levels: at 0.01 mbar (~102 km), the VMR varies between 0.33 ± 0.01 ppmv to 1.15 ± 0.05 ppmv, or a factor 3.5; at 0.03 mbar (~97 km), it varies from 0.35 ± 0.006 ppmv to 0.72 ± 0.005 ppmv, or a factor 2; at 0.1 mbar (~93 km), it varies from 0.33 ± 0.01 ppmv to 0.52 ± 0.02 ppmv, or a factor 1.6; at 0.32 mbar (~88 km), it varies from 0.09 ± 0.004 ppmv to 0.28 ± 0.02 ppmv, or a factor 3. The density gradient over time is steeper at the lowest pressure levels, and gets steeper again at the higher pressure level. After orbit 900 (October 2008) until orbit 2400 (November 2012), large short-term variations are observed at all pressure levels, higher than one order of magnitude, and a small decrease with time is observed, with a factor varying between 0.34 at 0.32 mbar (~88 km) and 1 at 0.1 mbar (~93 km).

As reported by many authors (Krasnopolsky and Pollack, 1994; Mills and Allen, 2007; Yung and DeMore, 1982; Yung et al., 2009), HCl plays a key role in the three principals chemical cycles, thats is, the sulfur oxidation, the CO_2 and the polysulfur cycles, and the above presented results show that further investigation is necessary for understanding reasons of such time and vertical variations and trends. For example comparing the SOIR results to the JPL/Caltech KINETICS 1D-photochemical model (see Table 2 of the companion paper Parkinson et al. (2014)) would help understanding and explaining these observations.

4.3. Fluoric acid

The good quality of the HF spectral fits is illustrated in Fig. 8. In this figure, four altitude levels are considered (99.3 km, 86.6 km, 79.7 km and 72.6 km), at which the R(1) HF line of the 1–0 band is clearly seen (4038.96 cm^{-1}, inside the black box); the other spectral structures are from the $00^02(1)$–$01^10(1)$ hot band of the CO_2 main isotopologue (HITRAN notations (Rothman et al., 2013)). All the number density profiles from the main isotopologue are presented in panel A of Fig. 9. The color code is the absolute latitude, such as in Fig. 1. The mean HF profiles are calculated for a width of the moving average box equal to ± 0.4 scale heights (see the definition in the Retrieval method section). The error bars are not given for the sake of clarity: they range between

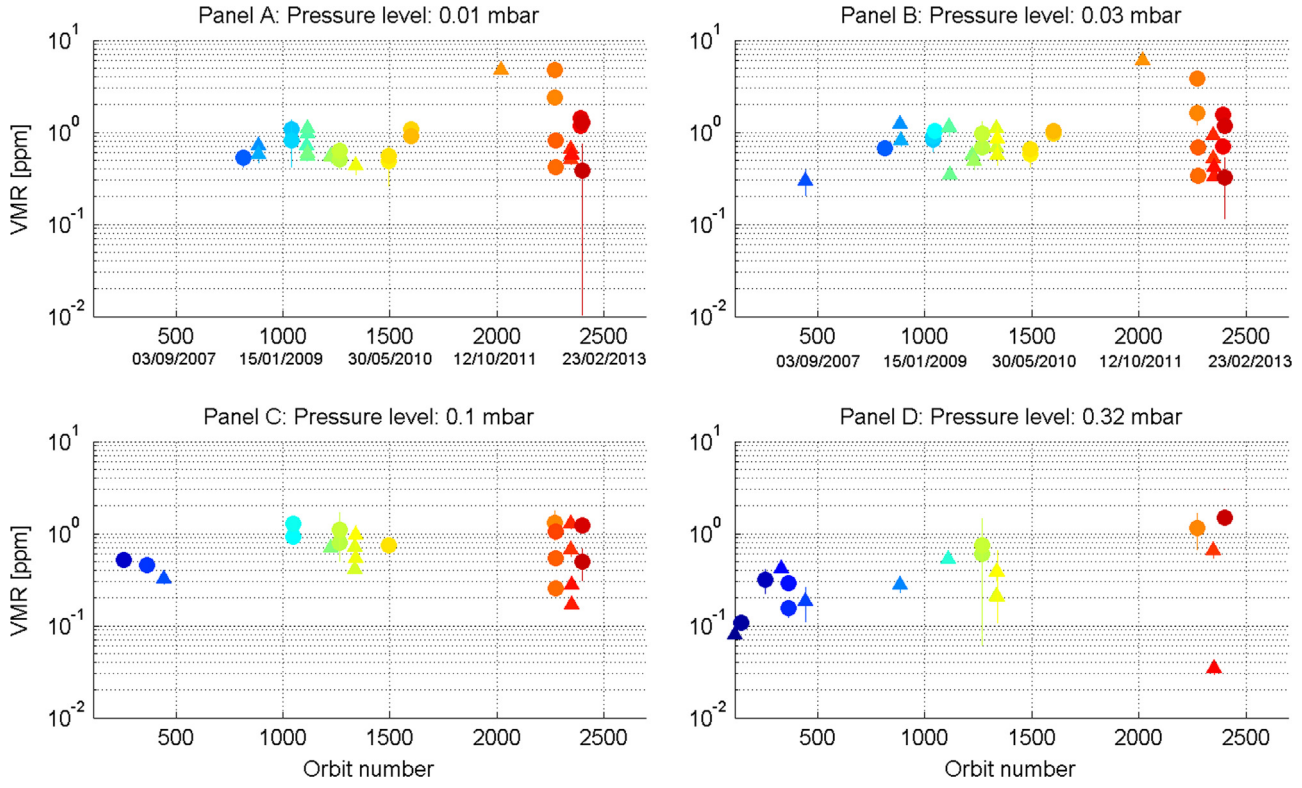

Fig. 6. Long-term variations of $H^{35}Cl$ and $H^{37}Cl$ for the equatorial region (0°–30°) at four pressure levels are presented: 0.01 mbar (~102 km) in Panel A, 0.03 mbar (~97 km) in Panel B, 0.1 mbar (~93 km) in Panel C and 0.32 mbar (~88 km) in Panel D. The color code is the orbit number. The error bars are the vertical bars. Circles are for morning measurements, while triangles are for evening ones.

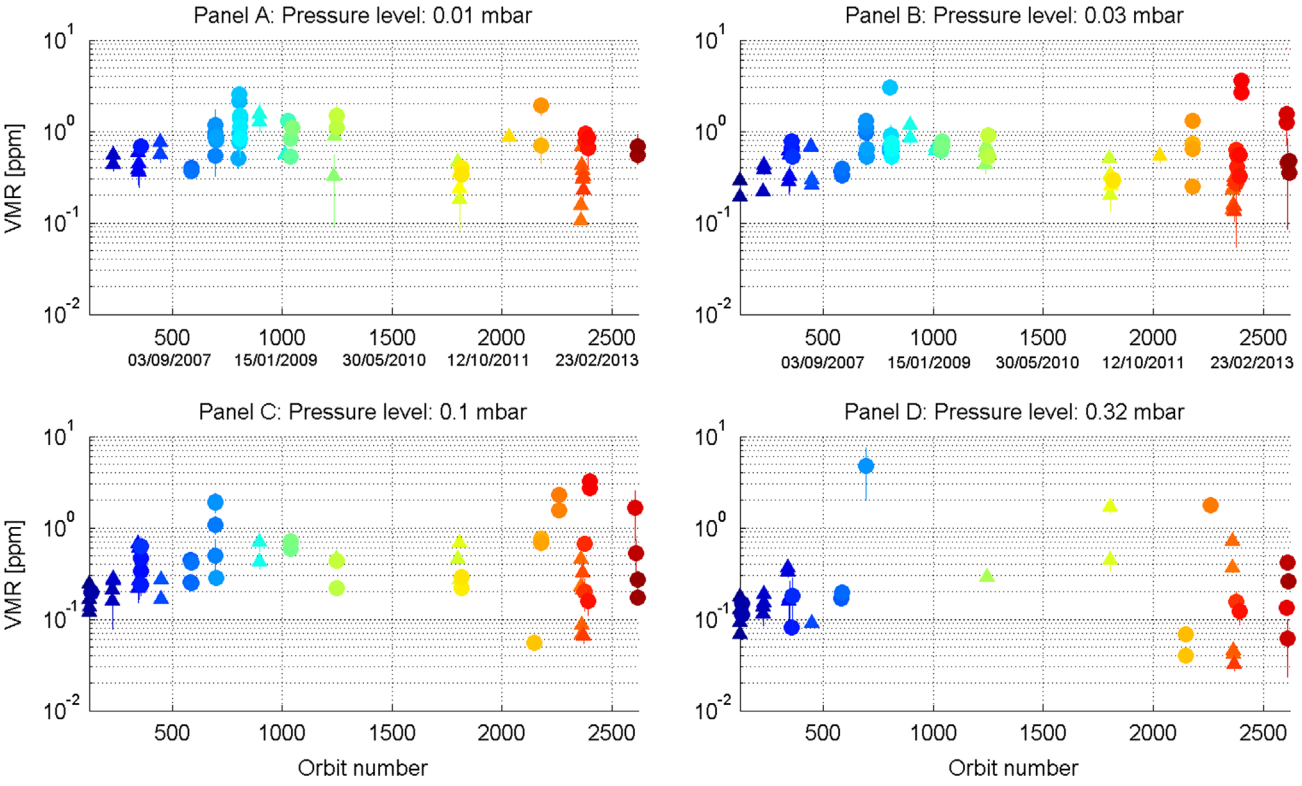

Fig. 7. Long-term variations of $H^{35}Cl$ and $H^{37}Cl$ for the polar region (80°–90°) at four pressure levels are presented: 0.01 mbar (~102 km) in Panel A, 0.03 mbar (~97 km) in Panel B, 0.1 mbar (~93 km) in Panel C and 0.32 mbar (~88 km) in Panel D. The color code is the orbit number. The error bars are the vertical bars. Circles are for morning measurements, while triangles are for evening ones.

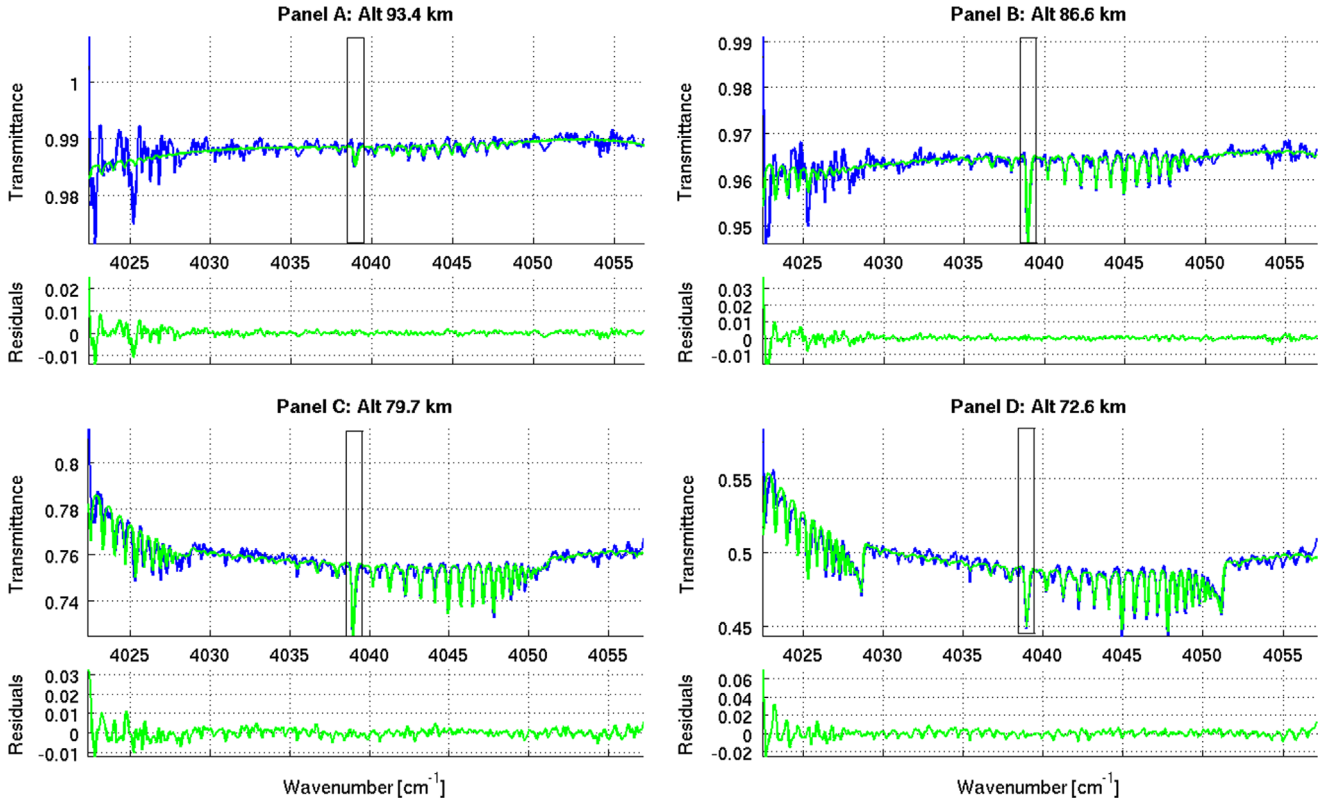

Fig. 8. Example of spectral fit of orbit 130.1 (29/08/2006) at four altitude levels (99.3 km in Panel A, 86.6 km in Panel B, 79.7 km in Panel C and 72.6 km in Panel D). In the top part of these panels, the measured spectra (order 180 bin 1) are in blue and the fitted spectra are in green. The HF absorption line is in the black box. The other spectral structures are from CO_2. The bottom part of each panel is the residuals of the fits.

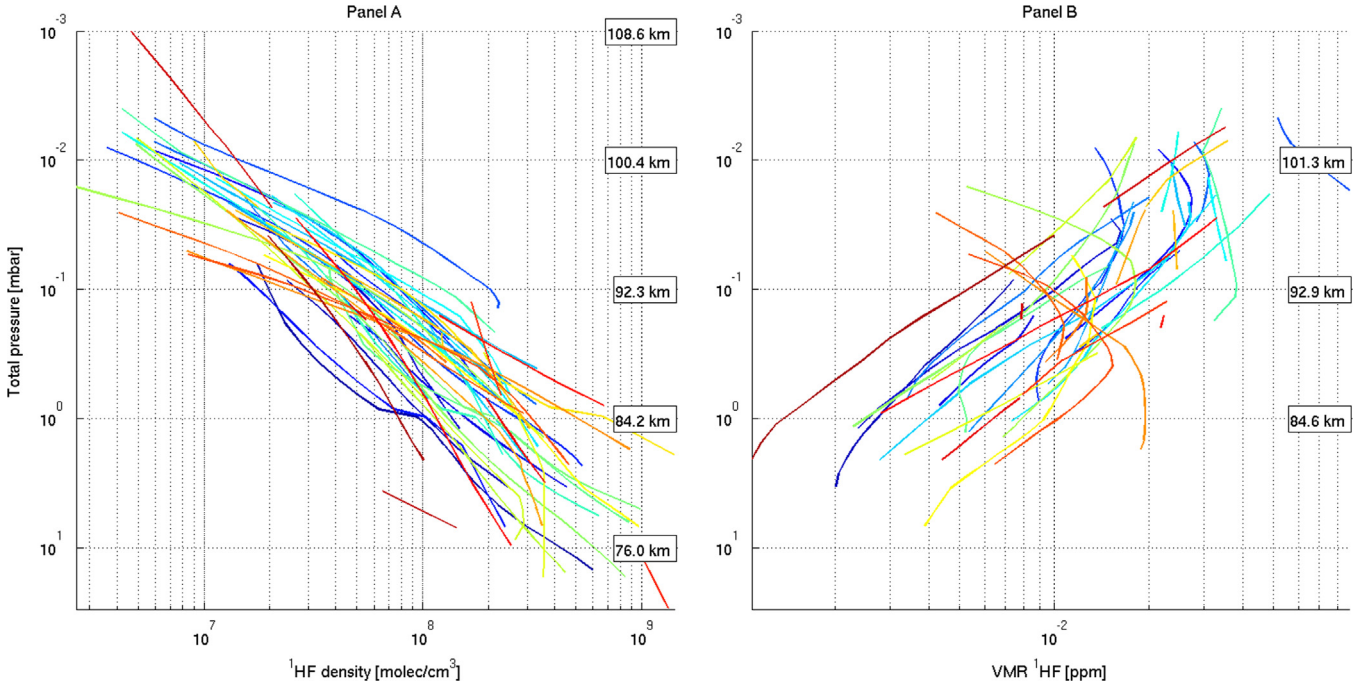

Fig. 9. HF number density profiles (panel A) and VMR profiles (panel B). The color code is the absolute latitude (blue to red for increasing absolute latitude). The number density profiles are given as a function of altitude; the VMR profiles are given as a function of pressure, the altitude is also shown in correlation with the pressure scale. The error bars are not displayed for sake of clarity. They vary between 10% and 100%, with a mean value of 15%.

10% and 100%, with an average value of 15%. As for HCl, the relative error does not directly depend on the altitude level, but on the signal to noise ratio. The number density profiles are given as a function of pressure, to remove the variations of the mean atmosphere (Mahieux et al., 2014a). The average geometric standard deviation of the CO_2 profiles equals to 2.2. The profiles cover the 75 to 110 km altitude

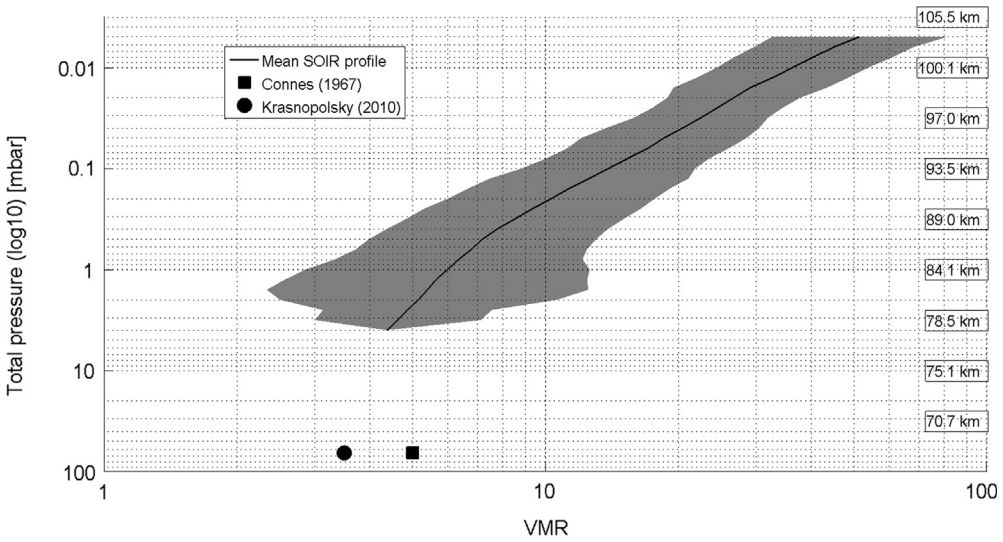

Fig. 10. Mean value of the HF VMR as a function of total pressure, for all latitudes combined. The altitude is also shown in correlation with the pressure scale. The weighted standard deviation is the colored shaded envelope.

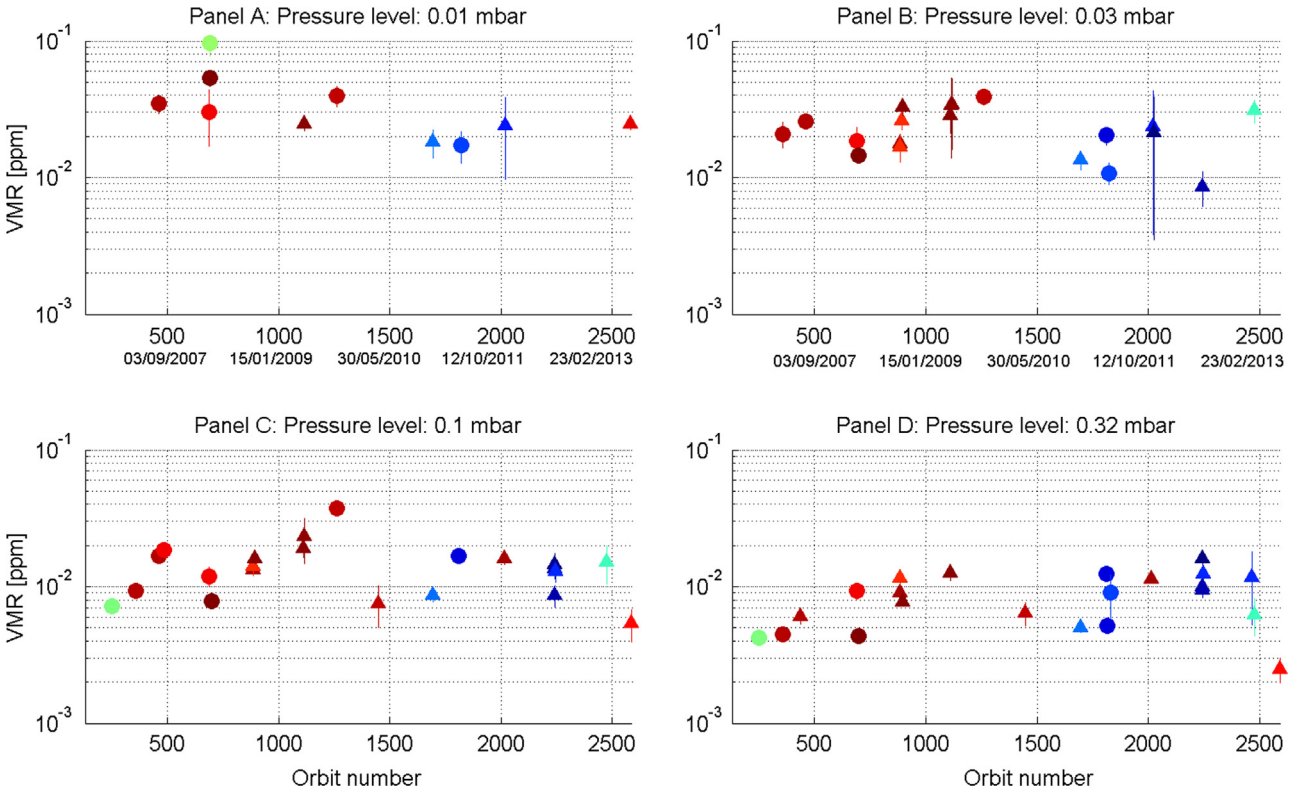

Fig. 11. Long-term variations of HF for all latitudes at four pressure levels are presented: 0.01 mbar (~100 km) in Panel A, 0.03 mbar (~97 km) in Panel B, 0.1 mbar (~94 km) in Panel C and 0.32 mbar (~89 km) in Panel D. The color code is the absolute latitude, blue for equatorial, red for polar. The error bars are the vertical bars. Circles are for morning measurements, while triangles are for evening ones.

region. The geometric standard deviation of the density varies between 1.4 and 2 with pressure, with an average value of 1.5. The corresponding VMR profiles are presented in panel B of the same figure, using the same color code; they are only calculated when a CO_2 profile is available at the same pressure level, as for HCl. A positive gradient with increasing altitude is observed in most of the profiles, while others show nearly constant or decreasing VMR profiles.

One mean HF profile is calculated for all latitudes and both sides of the terminator and is presented in Fig. 10. The mean HF VMR profile is also calculated as a function of the total pressure, to remove the variations of the mean atmosphere. The profile shows a positive exponential slope with increasing altitude. The mean VMR is equal to 5 ppbv $\pm$ 35% at 3.16 mbar (~80 km), 6 ppbv $\pm$ 52% at 1 mbar (~84 km), 14 ppbv $\pm$ 36% at 0.1 mbar (~94 km), 36 ppbv $\pm$ 33% at 0.01 mbar (~100 km) and 51 ppbv $\pm$ 37% at 0.005 mbar (~105 km). The SOIR mean VMR profile is compared to literature data. The value reported by Connes et al. (1967) above the cloud deck is not within the SOIR altitude sensitivity range: the HF lines are atmospherically saturated at these pressure levels. However, the value lies within the extrapolated SOIR standard deviation values at these pressure levels,

assuming that the slope of the HF VMR profile does not show any changes at higher pressure levels. Same conclusions can be drawn for the value measured by Krasnopolsky (2010) 4 decades later in the same altitude region (Fig. 10).

The time dependence of the HF VMR has also been investigated here. All latitudes and both sides of the terminator are considered together for this study, see Fig. 11 where the color code is the absolute latitude, circles are for morning side and triangles for evening side measurements, such as in Fig. 1. We observe a large short-term variability of the VMR at each pressure level as a function of time, up to one order of magnitude. At the lowest pressure level, 0.01 mbar (~100 km), a long-term trend is observed, with a decrease from 48 ± 2 ppbv in September 2006 (orbit 100) to 22 ± 1 ppbv in May 2013 (orbit 2500), that is, a factor 0.5. At 0.03 mbar (~97 km), the mean VMR also decreases from 23 ± 1 ppbv to 17.3 ± 1 ppbv, or a factor 0.7. Inversly, at higher pressure, the opposite is observed, with an increase from 12.9 ± 0.3 ppbv to 16.3 ± 0.4 ppbv the 0.1 mbar level (~94 km), or a factor 1.3, and even larger at the 0.32 mbar level (~89 km), with an increase from 5.5 ± 0.1 ppbv to 10.6 ± 0.2 ppbv or a factor 2 on the same period. This means that the mean vertical HF gradient varies with time.

HF is usually not considered in chemical models of the Venus atmosphere because of its low abundance and its low reactivity. We speculate that since its VMR shows vertical variations, latitudinal trends below 80 km and above 100 km, and long-term trends, HF might however play a role in the chemistry cycles of the Venus atmosphere. But, its abundance is much smaller than the one of HCl (by a factor 100) and chemical reactions involving HF could be slower than similar reactions involving HCl.

5. Conclusions

HCl is one of the important active species that plays a role in the major Venus chemical cycles (Krasnopolsky, 2012b; McElroy et al., 1973; Mills and Allen, 2007; Prinn, 1971; Yung and DeMore, 1982). HF is present in much lower concentration in the Venus atmosphere, with a volume mixing ratio usually a factor 100 smaller compared to HCl. In addition, HF photolysis begins at 180 nm where strong CO_2 absorption occurs on Venus and as a consequence would be less efficient than HCl photolysis, starting at 230 nm (Krasnopolsky et al., 2013). Usually HF is assumed to play a minor role in the Venus atmosphere chemistry; however this work indicates that it might play a role. Nevertheless, HCl and HF chemistries are expected to be broadly similar.

The SOIR instrument regularly sounds the Venus atmosphere using the solar occultation technique, and retrieves HCl and HF vertical profiles at both sides of the terminator, in the 70–115 km and 75–110 km regions, respectively. All latitudes from pole to pole are covered, with a lack of measurements in the 30°–60° North due to the satellite orbit. From the number density profiles derived using the ASIMAT algorithm, VMR profiles have been determined, using only the simultaneous CO_2 measurements. HCl VMR values between 0.40 ppmv (Krasnopolsky, 2012a; Young, 1972) and 0.76 ppmv (Iwagami et al., 2008) were reported above the cloud deck (between ~70 and ~74 km). At a pressure of 10 mbar (~74 km), we found values of 55 ppbv ± 134% (1-σ standard deviation) in the polar bin, one order of magnitude lower than the values reported in the literature. For HF, Krasnopolsky (2010) reported a constant VMR of 3.5 ppbv near the cloud top, for latitudes between ± 60°. The mean value in this study at 3.16 mbar (~80 km) is about 5 ppbv ± 35%. Altogether, VMR values for both halides in this work are smaller than those in previous studies.

The VMR profiles of both hydrogen halides show a positive gradient in the 4 mbar (~78 km) to 0.02 mbar (~98 km), which is not expected from models (Krasnopolsky, 2012b) that predict constant VMR profiles in the SOIR sensitivity altitude range. Sandor and Clancy (2012) even reported a negative gradient of the HCl VMR with altitude, in the 65–125 km region, yet at other local solar times. However, the HCl VMR derived in this study is nearly constant for pressure ranges larger than 4 mbar (lower than ~78 km) and lower than 0.02 mbar (larger than ~98 km). It seems difficult to explain the positive gradient at this stage but it should be noted that a positive gradient has also been observed for SO_2 (Belyaev et al., 2012; Mahieux et al., 2014b; Moullet et al., 2013) and HCl and SO_2 are linked by chemistry in the Venus mesosphere.

The long-term variations were investigated for both species, and the latitude variations were addressed for HCl. The latest does not present large latitude variations for the latitudes bins considered in this work. The short-term variations are dominant at all latitudes. Long-term variations for constant pressure levels in the equatorial region (0°–30°) show that the HCl VMR at the lowest pressure level, 0.32 mbar (~88 km), followed a constant exponential increase of a factor nearly equal to 3. In the polar regions, an important exponential increase was observed between August 2006 and October 2008, varying in strength with the pressure levels, followed by a weak decrease until November 2012, also pressure dependent. The chemical, physical or dynamical effects producing these time dependent vertical gradients are unknown. The HF long-term variations show same order logarithmic VMR gradient with time in the 0.01 mbar (~100 km) to 0.32 mbar (~89 km) region. However latitudinal variations of HCl and long-term variations of both HCl and HF VMR are about a factor 2 to 3, while differences in VMR related to the pressure are lower than one order of magnitude and on the short-term the VMR can vary up to one order of magnitude for a given pressure level.

Acknowledgments

Venus Express is a planetary mission from the European Space Agency (ESA). We wish to thank all ESA members who participated in the mission, in particular, H. Svedhem and D. Titov. We thank our collaborators at IASB-BIRA (Belgium), LATMOS (France), and IKI (Russia). We thank CNES, CNRS, Roskosmos, and the Russian Academy of Science. The research program was supported by the Belgian Federal Science Policy Office and the European Space Agency (ESA, PRODEX program, contracts C 90268, 90113, and 17645). A. Mahieux thanks the FNRS for the position of "chargé de recherches". We acknowledge the support of the "Interuniversity Attraction Poles" program financed by the Belgian government (Planet TOPERS). The research leading to these results has received funding from the European Union Seventh Framework Program (FP7/2007–2013) under grant agreement n°606798 (EuroVenus).

References

Belyaev, D., Montmessin, F., Bertaux, J.L., Mahieux, A., Fedorova, A., Korablev, O., Marcq, E., Yung, Y., Zhang, X., 2012. Vertical profiling of SO_2 and SO above Venus' clouds by SPICAV/SOIR solar occultations. Icarus 217, 740–751.

Bertaux, J.L., Nevejans, D., Korablev, O., Villard, E., Quémerais, E., Neefs, E., Montmessin, F., Leblanc, F., Dubois, J.P., Dimarellis, E., Hauchecorne, A., Lefevre, F., Rannou, P., Chaufray, J.Y., Cabane, M., Cernogora, G., Souchon, G., Semelina, F., Reberac, A., Van Ransbeek, E., Berkenbosch, S., Clairquin, R., Muller, C., Forget, F., Hourdin, F., Talagrand, O., Rodin, A., Fedorova, A., Stepanov, A., Vinogradov, A., Kiselev, A., Kalinnikov, Y., Durry, G., Sandel, B., Stern, A., Gérard, J.C., 2007. SPICAV on Venus Express: Three spectrometers to study the global structure and composition of the Venus atmosphere. Planet. Space Sci. 55, 1673–1700.

Connes, P., Connes, J., Benedict, W.S., Kaplan, L., 1967. Traces of HCl and HF in the atmosphere of Venus. Astrophys. J. 147, 1230–1237.

Fedorova, A., Korablev, O., Vandaele, A.C., Bertaux, J.L., Belyaev, D., Mahieux, A., Neefs, E., Wilquet, V., Drummond, R., Montmessin, F., Villard, E., 2008. HDO and H_2O vertical distributions and isotopic ratio in the Venus mesosphere by solar occultation at Infrared spectrometer onboard Venus Express. J. Geophys. Res., 113. http://dx.doi.org/10.1029/2008JE003146.

Hedin, A.E., Niemann, H.B., Kasprzak, W.T., 1983. Global empirical model of the Venus thermosphere. J. Geophys. Res. 88, 73–83.
Iwagami, N., Ohtsuki, S., Tokuda, K., Ohira, N., Kasaba, Y., Imamura, T., Sagawa, H., Hashimoto, G.L., Takeuchi, S., Ueno, M., Okumura, S., 2008. Hemispheric distributions of HCl above and below the Venus' clouds by ground-based 1.7 mm spectroscopy. Planet. Space Sci. 56, 1424–1434.
Krasnopolsky, V., 2012a. Observation of DCl and upper limit to NH_3 on Venus. Icarus 219, 244–249.
Krasnopolsky, V., Pollack, J.B., 1994. H_2O-H_2SO_4 system in Venus' clouds and OCS, CO and H_2SO_4 profiles in Venus troposphere. Icarus 109, 58–78.
Krasnopolsky, V.A., 2010. Spatially-resolved high-resolution spectroscopy of Venus. 1. Variations of CO_2, CO, HF, and HCl at the cloud tops. Icarus 208, 539–547.
Krasnopolsky, V.A., 2012b. A photochemical model for the Venus atmosphere at 47–112 km. Icarus 218, 230–246.
Krasnopolsky, V.A., Belyaev, D.A., Gordon, I.E., Li, G., Rothman, L.S., 2013. Observations of D/H ratios in H_2O, HCl, and HF on Venus and new DCl and DF line strengths. Icarus 224, 57.
Mahieux, A., 2011. Inversion of the Infrared Spectra Recorded by the SOIR Instrument on Board Venus Express (PhD Thesis). Université Libre de Bruxelles, Belgium.
Mahieux, A., Berkenbosch, S., Clairquin, R., Fussen, D., Mateshvili, N., Neefs, E., Nevejans, D., Ristic, B., Vandaele, A.C., Wilquet, V., Belyaev, D., Fedorova, A., Korablev, O., Villard, E., Montmessin, F., Bertaux, J.L., 2008. In-flight performance and calibration of SPICAV/SOIR on-board Venus Express. Appl. Opt. 47, 2252–2265.
Mahieux, A., Vandaele, A.C., Bougher, S.W., Drummond, R., Robert, S., Chamberlain, S., Wilquet, V., Piccialli, A., Montmessin, F., Tellmann, S., Pätzold, M., Häusler, B., Bertaux, J.L., 2014a. Update of the Venus density and temperature profiles at high altitude measured by SOIR on board Venus Express. Planet. Space Sci, in press.
Mahieux, A., Vandaele, A.C., Drummond, R., Robert, S., Wilquet, V., Fedorova, A., Bertaux, J.L., 2010. Densities and temperatures in the Venus mesosphere and lower thermosphere retrieved from SOIR onboard Venus Express: retrieval technique. J. Geophys. Res. 115, http://dx.doi.org/10.1029/2010JE003589.
Mahieux, A., Vandaele, A.C., Robert, S., Wilquet, V., Drummond, R., Belyaev, D., Bertaux, J.L., 2014b. Venus mesospheric sulfur dioxide measurement retrieved from SOIR on board Venus Express. Planet. Space Sci , http://dx.doi.org/10.1016/j.pss.2014.12.011, in press.
Mahieux, A., Vandaele, A.C., Robert, S., Wilquet, V., Drummond, R., Montmessin, F., Bertaux, J.L., 2012. Densities and temperatures in the Venus mesosphere and lower thermosphere retrieved from SOIR on board Venus Express: carbon dioxide measurements at the Venus terminator. J. Geophys. Res., 117. http://dx.doi.org/10.1029/2012JE004058.
Mahieux, A., Wilquet, V., Drummond, R., Belyaev, D., Fedorova, A., Vandaele, A.C., 2009. A new method for determining the transfer function of an acousto optical tunable filter. Opt. Express 17, 2005–2014.
McElroy, M.B., Sze, N.D., Yung, Y.L., 1973. Photochemistry of the Venus atmosphere. J. Atmos. Sci. 30, 1437–1447.
Mills, F.P., Allen, M., 2007. A review of selected issues concerning the chemistry in Venus' middle atmosphere. Planet. Space Sci. 55, 1729–1740.
Moullet, A., Moreno, R., Encrenaz, T., Lellouch, E., Fouchet, T., 2013. Submillimeter spectroscopy of Venus's atmosphere with ALMA: CO, HDO, and sulfur species. DPS (Division for Planetary Sciences) Forty Fifth Annual Meeting. Boulder, Colorado.
Nevejans, D., Neefs, E., Van Ransbeeck, E., Berkenbosch, S., Clairquin, R., De Vos, L., Moelans, W., Glorieux, S., Baeke, A., Korablev, O., Vinogradov, I., Kalinnikov, Y., Bach, B., Dubois, J.P., Villard, E., 2006. Compact high-resolution space-borne echelle grating spectrometer with AOTF based on order sorting for the infrared domain from 2.2 to 4.3 μm. Appl. Opt. 45, 5191–5206.
Parkinson, C., Yung, Y., Esposito, L., Gao, P., Bougher, S.W., Hirtzig, M., 2014. Photochemical control of the distribution of Venusian water and comparison to Venus Express SOIR observations. Planet. Space Sci, in press.
Prinn, R.G., 1971. Photochemistry of HCl and other minor constituents in the atmosphere of Venus. J. Atmos. Sci. 28, 1058–1068.
Rodgers, C.D., 2000. Inverse Methods for Atmospheric Sounding: Theory and Practice. University of Oxford, Singapore.
Rothman, L.S., Gordon, I.E., Babikov, Y., Barbe, A., Benner, D.C., Bernath, P.F., Bizzocchi, L., Boudon, V., Brown, L.R., Campargue, A., Chance, K.V., Cohen, E.A., Coudert, L.H., Devi, V.M., Drouin, B.J., Fayt, A., Flaud, J.-M., Gamache, R., Harrison, J.J., Hartmann, J.M., Hill, C., Hodges, J., Jacquemart, D., Jolly, A., Lamouroux, J., LeRoy, R.J., Li, G., Long, D.A., Lyulin, O.M., Mackie, C.J., Massie, S., Mikhailenko, S., Muller, H.S.P., Naumenko, O., Nikitin, A., Orphal, J., Perevalov, V., Perrin, A., Polovtseva, E.R., Richard, C., Smith, M.A.H., Starikova, E., Sung, K., Tashkun, S., Tennyson, J., Toon, G., Tyuterev, V.G., Wagner, G., 2013. The HITRAN2012 molecular spectroscopic database. J. Quant. Spectrosc. Radiat. Transf. 130, 4.
Sandor, B., Clancy, R.T., 2012. Observations of HCl altitude dependence and temporal variation in the 70–100 km Mesosphere of Venus. Icarus 220, 618–626. http://dx.doi.org/10.1016/j.icarus.2012.05.016.
Titov, D.V., Svedhem, H., Koschny, D., Hoofs, R., Barabash, S., Bertaux, J.L., Drossart, P., Formisano, V., Haüsler, B., Korablev, O., Markiewicz, W., Nevejans, D., Pätzold, M., Piccioni, G., Zhang, T., Merritt, D., Witasse, O., Zender, J., Accomazzo, A., Sweeney, M., Trillard, D., Janvier, M., Clochet, A., 2006. Venus Express science planning. Planet. Space Sci. 54, 1279–1297.
Toth, R.A., Darnton, L.A., 1974. Linewidths of HCl broadened by CO_2 and N_2 and CO broadened by CO_2. J. Mol. Spectrosc. 49, 100–105.
Tudorie, M., Földes, T., Vandaele, A.C., Vander Auwera, J., 2012. CO_2 pressure broadening and shift coefficients for the 1–0 band of HCl and DCl J. Quant. Spectrosc. Radiat. Transf. 113, 1092–1101.
Vandaele, A.C., De Mazière, M., Drummond, R., Mahieux, A., Neefs, E., Wilquet, V., Korablev, O., Fedorova, A., Belyaev, D., Montmessin, F., Bertaux, J.L., 2008. Composition of the Venus mesosphere measured by SOIR on board Venus Express. J. Geophys. Res., 113. http://dx.doi.org/10.1029/2008JE003140.
Vandaele, A.C., Mahieux, A., Robert, S., Berkenbosch, S., Clairquin, R., Drummond, R., Letocart, V., Neefs, E., Ristic, B., Wilquet, V., Colomer, F., Belyaev, D., Bertaux, J.L., 2013. Improved calibration of SOIR/Venus Express spectra. Opt. Express 21, 21148.
Vandaele, A.C., Mahieux, A., Robert, S., Drummond, R., Wilquet, V., Bertaux, J.L., 2014. Carbon monoxide short term variability observed on Venus with SOIR/VEX. Planet. Space Sci., http://dx.doi.org/10.1016/j.pss.2014.12.012, in press.
von Zahn, U., Fricke, K.H., Hunten, D.M., Krankowsky, D., Mauersberger, K., Nier, A.O., 1980. The upper atmosphere of Venus during morning conditions. J. Geophys. Res. 85, 7829–7840.
Wilquet, V., Drummond, R., Mahieux, A., Robert, S., Vandaele, A.C., Bertaux, J.L., 2012. Optical extinction due to aerosols in the upper haze of Venus: four years of SOIR/VEX observations from 2006 to 2010. Icarus 217, 875–881.
Wilquet, V., Fedorova, A., Montmessin, F., Drummond, R., Mahieux, A., Vandaele, A.C., Villard, E., Korablev, O., Bertaux, J.L., 2009. Preliminary characterization of the upper haze by SPICAV/SOIR solar occultation in UV to mid-IR onboard Venus Express. J. Geophys. Res., 114. http://dx.doi.org/10.1029/2008JE003186.
Young, L., 1972. High resolution spectra of Venus: a review. Icarus 17, 632–658.
Yung, Y.L., DeMore, W.B., 1982. Photochemistry of the stratosphere of Venus: implications for atmospheric evolution. Icarus 51, 199–247.
Yung, Y.L., Liang, M.C., Jiang, X., Shia, R.L., Lee, C., Be´zard, B., Marcq, E., 2009. Evidence for carbonyl sulfide (OCS) conversion to CO in the lower atmosphere of Venus. J. Geophys. Res. 114, E00B34. http://dx.doi.org/10.1029/2008JE003094.
Zasova, L.V., Ignatiev, N., Khatuntsev, I., Linkin, V., 2007. Structure of the Venus atmosphere. Planet. Space Sci. 55, 1712–1728.